

## IMAGE ANALYTICAL DETERMINATION OF THE SPHERULITE GROWTH IN POLYPROPYLENE COMPOSITES

ALI MOGHISEH<sup>1</sup>, KATJA SCHLADITZ<sup>✉,1</sup>, ALOIS K. SCHLARB<sup>2,3</sup>, BUNCHA SUKSUT<sup>4</sup>

<sup>1</sup>Fraunhofer-Institute for Industrial Mathematics ITWM, Kaiserslautern, Germany; <sup>2</sup>Chair of Composite Engineering, University of Kaiserslautern, Germany; <sup>3</sup>State Research Center OPTIMAS, University of Kaiserslautern, Germany; <sup>4</sup>King Mongkut's University of Technology North Bangkok, Rayong Campus, Rayong, Thailand

e-mail: ali.moghiseh@itwm.fraunhofer.de, katja.schladitz@itwm.fraunhofer.de, alois.schlarb@mv.uni-kl.de, buncha.s@eat.kmutnb.ac.th

(Received January 22, 2018; revised April 23, 2018; accepted April 27, 2018)

### ABSTRACT

Measuring the growth of spherulites in semi-crystalline thermoplastics helps to control and optimize industrial manufacturing processes of these materials. The growth can be observed in cross polarized images, taken at several time steps. The diameters of the spherulites are however measured manually in each step. Here, two approaches for replacing this tedious and time consuming method by automatic image analytic measurements are introduced. The first approach segments spherulites by finding salient 5x5 pixel patches in each time frame. Combining the information from all time frames into a 3D image yields the spherulites by a maximal flow graph cut in 3D. The growth is then measured by homography measurement. The second approach is closer to the manual method. Based on the Hough transform, spherulites are identified by their circular outline. The growth is then measured by comparing the radii of the least moving circles. The pros and cons of these methods are discussed based on synthetic image data as well as by comparison with manually measured growth rates.

Keywords: Hough transform, homography estimation

### INTRODUCTION

The performance characteristics of semi-crystalline thermoplastic products are determined by their intrinsic properties such as molecular orientation, supramolecular morphology, and residual stresses. These parameters are determined by the materials themselves and the processing conditions. In principle, during the manufacturing of products from semi-crystalline thermoplastics during cooling from a quiescent melt, spherical supramolecular structures, in short spherulites are formed. The bottleneck for the cycle time in the processing of these materials using industrial manufacturing processes such as injection molding is the cooling phase from the melt, respectively the nucleation rate and the spherulite growth rate. Therefore, it is extremely important to identify this behavior for different plastics and their composites.

As early as 1995, (Plummer and Kausch) used images of samples between cross polarizers to study the spherulite growth in polyoxymethylene image analytically. Their method works however for very low spherulite area fractions (1%) only, as it relies on

object labelling. (Hernández-Sánchez and Carrillo-Escalante, 2009) correlate average gray values of cross polarized images with the spherulite growth in polylactic acid. The measurement is however not a local one and moreover requires a high calibration effort. Even more recently, spherulite radii are still measured manually from image data (De Santis *et al.*, 2014; Nomai *et al.*, 2015). However, this procedure is extremely time consuming.

Here, we introduce two approaches for automatic measurement of spherulite growth based on image data. The algorithmic background of both is shortly summarized. Their results are compared to those from manual measurements.

### MATERIALS AND METHODS

#### MATERIALS AND SAMPLE PREPARATION

Polypropylene and a composite of polypropylene (PP) and microfibrillated cellulose (MFC) were selected as test materials and used to prepare 25/±5 µm thick

films under the conditions described in (Thanomchat *et al.*, 2014). As polymer matrix, a commercially available polypropylene (PP HD120MO, Borealis GmbH, Burghausen, Germany) was used. The micellar cellulose was prepared at Chulalongkorn University (Department of Materials Science, Faculty of Science, Chulalongkorn University, Bangkok, Thailand) as described in (Thanomchat *et al.*, 2014).

## EXPERIMENTS AND MANUAL SIZE MEASUREMENT

A stack (glass substrate, polymer/composite thin section ( $25/\pm 5 \mu\text{m}$ ), cover slip) was fixed at a hot stage (LTS 420, Linkam Scientific Instruments, Surrey, England) under a light microscope (ECLIPSE LV100, Nikon GmbH, Düsseldorf, Germany). The samples were heated to  $200 \text{ }^\circ\text{C}$  at a rate of  $20 \text{ K/min}$  and held for 3 min at this temperature. Then, for isothermal crystallization, the samples were cooled at the rate of  $20 \text{ K/min}$  to various given crystallization temperatures ( $130 \text{ }^\circ\text{C}$ ,  $132 \text{ }^\circ\text{C}$ , and  $134 \text{ }^\circ\text{C}$ ) and held constant until completion of crystallization was observed. The development of the spherulitic structure was detected under polarized light and recorded using a CCD camera. The radial growth rate of the spherulites was calculated using the recorded movies based on the size of PP spherulites as a function of time. Five spherulites of each sample were characterized. A radius of each was measured from a manually chosen center to the outside edge. Each crystallization experiment was performed at least three times in order to verify the reproducibility of the experiment.

## IMAGE ANALYTIC GROWTH BY HOMOGRAPHY ESTIMATION

The first step for this growth rate analysis method is to segment the spherulites in each frame. To this end, foreground candidates are detected as the set of salient  $5 \times 5$  pixel patches following (Margolin *et al.*, 2013). Here “salient” defines patches differing significantly from the “average patch”. A model for the background

patches form the overwhelming majority. First the average patch is determined, subsequently the principal components are analyzed. Finally being distinct is measured by the  $L_1$ -distance to the average patch in the coordinate system given by the principal components. The thus derived score for being foreground is multiplied with a measure for color deviation on superpixels. For details see (Margolin *et al.*, 2013). The resulting stack of images with the foreground-score as gray values is interpreted as a 3D image and segmented by a maximal flow graph cut in 3D assuming 26-connectivity. An exemplary segmentation result is shown in Fig. 1.

Based on this segmentation, local growth is estimated for each pair of consecutive frames: Objects are labelled interpreting the pair as a 3D image. Then the contours of the corresponding objects in 2D are deduced from the local gradients in x and y directions. For each pixel in a contour, its counterpart in the consecutive frame is found as the one closest to it. Based on these pairs of points, the homography (projective transformation) mapping the previous into the current frame is estimated robustly using the algorithm from (Hartley and Zisserman, 2003). The correspondences are corrected accordingly. This algorithm results in a table holding the local growth in the sense of the homography moving the object (edge) in the previous frame into the corresponding one in the current frame. In particular, the growth estimation is based only on one pair of frames at a time as objects are not tracked.

For comparison with the manual measurements as well as the other method described below, the derived information on the growth from one time step to the next are post-processed: As in the manual method, five objects are picked. Here, those containing the most pixels are chosen. The growth for each object is the mean distance of the corresponding edge point pairs belonging to this object. Finally the growth for the current time step is calculated as the weighted mean over the growths of the five picked objects, where the weights are the edge lengths in number of pixels.

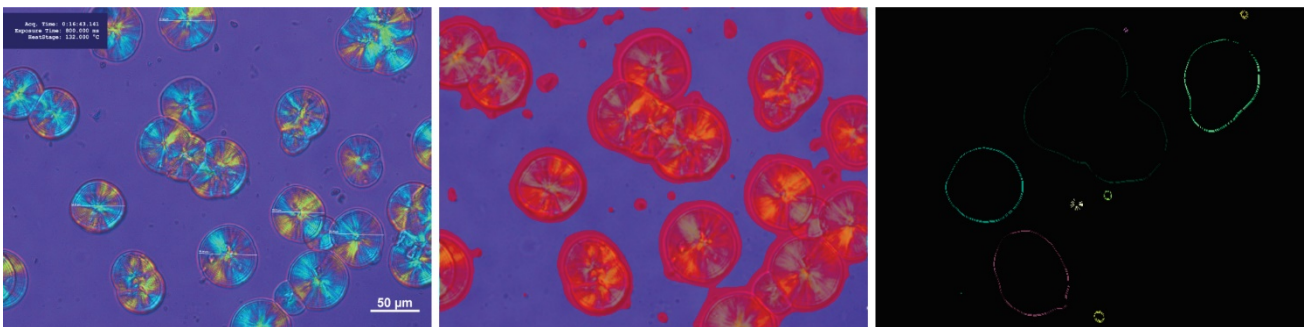


Fig. 1. Left: Original. Center: Detected foreground with red overlay. Right: Growth patterns.

We validated the method using synthetic data. A Boolean model (*see e.g.*, Stoyan, Kendall, Mecke, 1998) was simulated in the observation window and the circles grew randomly from time step to time step. Altogether, three times five sequences of 40 time steps each were generated using three different sets of parameters  $p_i$ ,  $i = 1, 2, 3$ . The numbers of circles are discretely evenly distributed on the natural numbers in the interval  $[15, 25]$  for  $i = 1, 2$  and  $[25, 35]$  for  $i = 3$ . The radial growth is uniformly distributed in the intervals  $[0.575, 0.975]$  for  $i = 1$  and  $3$  and in  $[0.3, 1.2]$  for  $i = 2$ . Thus, the mean radial growth is  $0.75 \mu\text{m}$  per time step, corresponding to  $4.41$  pixels at nominal resolution  $0.17 \mu\text{m}$  as in the real image data. Results are shown in Table 1.

### IMAGE ANALYTIC GROWTH BY HOUGH TRANSFORM

Our second approach is based on the Hough transform for finding circles in 2D. The original RGB color images are converted to gray value images by simply taking the mean of the three color channels. Then the most pronounced ten circles are detected using the Hough transform for finding circles. Here, we apply the algorithm by (Mosaliganti *et al.*, 2009). Roughly speaking, this algorithm works in the following way: The edge pixels given by the gradient image “vote” for centers of circles they might be contained in. This voting is repeated for all radii within a suitable interval. Finally, the most likely centers and corresponding radii are chosen.

Geometrically described, the transformation consi-

ders in each edge pixel a line through this pixel in gradient direction. Then for all pixels on this line with distance to the edge pixel within the given radius range, the corresponding gray value in the voting image is increased by 1. The image containing the votes as pixel gray values is called the Hough map. After all edge pixels are processed, the Hough map features the candidates for centers of circles as bright points. Thus, the first circle center is the pixel with the maximum gray value in the Hough map. We remove it and its neighborhood from the Hough map and search for the second global maximum. This process is repeated for the predefined number of circles we are looking for. Here, 10 is chosen as a compromise between finding this number of strongly pronounced circles at all and ensuring with high probability that five out of them can be observed from first to last frame.

Fig. 2 shows examples with found circles overlaid in green. The algorithm results in a list of centers and radii. Thus originally, the found circles are not tracked from time step to time step. To estimate the growth  $g_i$  from time  $t_i$  to  $t_{i+1}$ , the five least moving centers out of the 10 found ones are considered. A pair of circle centers  $C_i, C_{i+1}$  from consecutive time steps  $t_i$  to  $t_{i+1}$  is accepted to match as long as distance  $(C_i, C_{i+1}) < R_i/2$ , where  $R_i$  is the spherulite radius as deduced from the growth till  $t_i$ . That is,  $R_0 = 0$  and  $R_i = \sum g_j, j \leq i$ . The growth  $g_{i+1}$  is finally obtained as the mean over the five picked circles weighted by edge length. If less than five matching circles are found, then the remaining values are averaged.

Table 1. *Weighted mean growth rates estimated by the homography method for the simulated samples. The measured growths are averaged over all time steps. The homography method underestimates the growth systematically. The deviation is however smaller than one pixel.*

	Mean #cones	Mean growth ( $\mu\text{m}$ )	Growth max deviation ( $\mu\text{m}$ )	Estimated growth ( $\mu\text{m}$ )	Relative error (%)
20_0p3_0p75_seq1	20	0.75	0.3	0.69	8.6
20_0p3_0p75_seq2	20	0.75	0.3	0.71	5.8
20_0p3_0p75_seq3	20	0.75	0.3	0.68	9.6
20_0p3_0p75_seq4	20	0.75	0.3	0.73	3.0
20_0p3_0p75_seq5	20	0.75	0.3	0.69	7.5
20_0p6_0p75_seq1	20	0.75	0.6	0.62	17.7
20_0p6_0p75_seq2	20	0.75	0.6	0.69	8.2
20_0p6_0p75_seq3	20	0.75	0.6	0.65	13.3
20_0p6_0p75_seq4	20	0.75	0.6	0.70	6.2
20_0p6_0p75_seq5	20	0.75	0.6	0.67	10.9
30_0p3_0p75_seq1	20	0.75	0.3	0.70	6.5
30_0p3_0p75_seq2	20	0.75	0.3	0.72	4.4
30_0p3_0p75_seq3	20	0.75	0.3	0.70	7.3
30_0p3_0p75_seq4	20	0.75	0.3	0.68	9.2
30_0p3_0p75_seq5	20	0.75	0.3	0.71	5.0

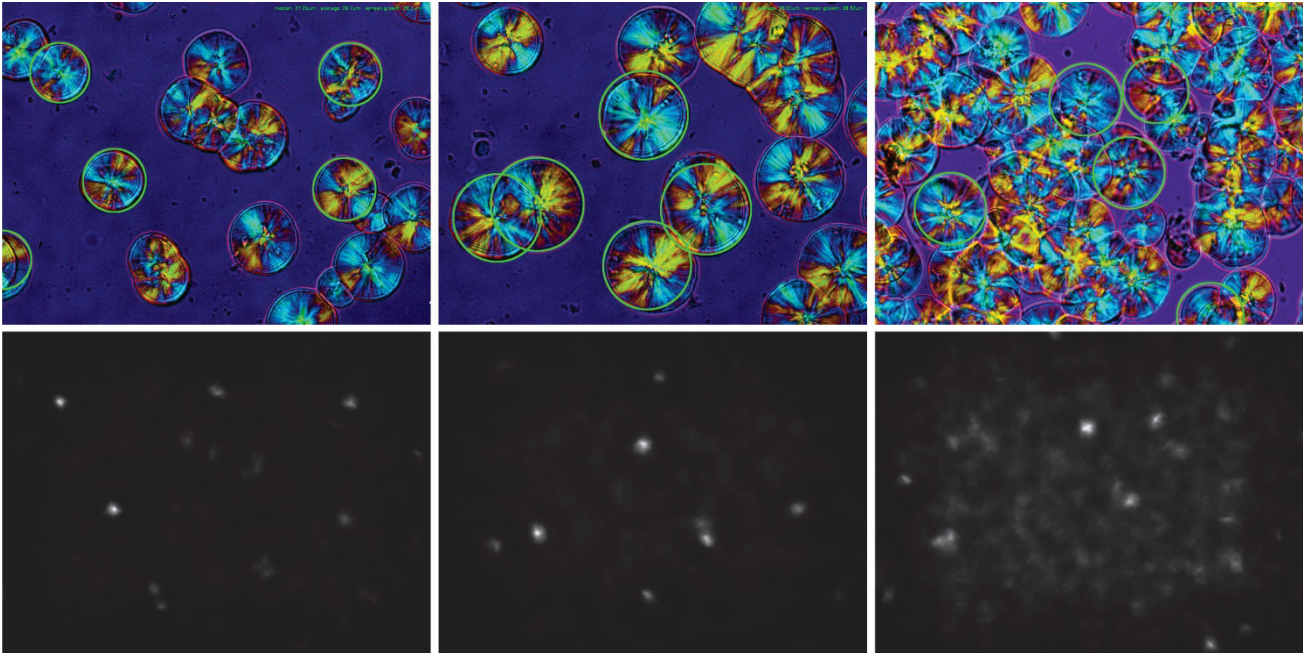


Fig. 2. Examples for the Hough circle method. Detected circles are overlaid in green over the original color images. The bottom row shows the corresponding Hough maps. Bright spots indicate very likely circle centers.

## RESULTS

Comparing the two image analytic and the manual measurements is not at all straightforward as they yield different results (diameters versus growth rates) that are differently weighted (number of selected circles versus number of corresponding edge pixels in consecutive frames). In order to compare as just as possible, we decided to weight all measured growth rates with the corresponding edge lengths. Exemplary results are shown in Fig. 3. Mean growth rates and relative measurement errors are summarized in Table 2.

The homography estimation approach works well for low object numbers and low spherulite area fraction. That is, in early growth stages. With growing area fraction, the estimation results deteriorate, due to the declining number of corresponding pixel pairs. The

Hough transform approach is very close to the manual measurement as it picks nicely defined circles as does the manual operator. Moreover, results are rather stable as neither pre-processing nor segmentation are needed. It is able to deal with clusters of spherulites. However, as soon as the shape of the spherulites deviates, the size is underestimated as the algorithm finds the inscribed circle, *e.g.*, of elliptical objects. Moreover, the circles in one frame are neither connected to the preceding nor the succeeding one.

The PP 4% MFC samples are particularly hard for both algorithms as the images contain agglomerates as visible, *e.g.*, the marked areas in Fig. 4. Moreover, they contain many spherulites, resulting in a high spherulite area fraction in later time steps, a disadvantage for the homography estimation.

Table 2. Weighted mean growth for all methods and nine samples. The measured growths are averaged over all time steps. Deviation of the results obtained by homography estimation is significantly higher. However, this is due to the fact that in the absence of better criteria, the manual measurement is taken as the “ground truth” here.

pp (%)	Temperature (°C)	Manually measured ( $\mu\text{m}$ )	Hough Circle ( $\mu\text{m}$ )	Rel diff (%)	Homography estimation ( $\mu\text{m}$ )	Rel diff (%)
0	130	1.334	1.258	5.7	1.052	21.2
0	132	0.880	0.859	2.3	0.849	3.5
0	134	0.626	0.608	2.8	0.520	16.9
1	130	1.410	1.286	8.8	1.222	13.3
1	132	0.940	0.806	14.3	0.774	17.7
1	134	0.634	0.616	2.9	0.528	16.8
4	130	1.529	1.559	2.0	1.036	32.2
4	132	0.938	0.893	4.9	0.698	25.6
4	134	0.636	0.584	8.0	0.383	39.8

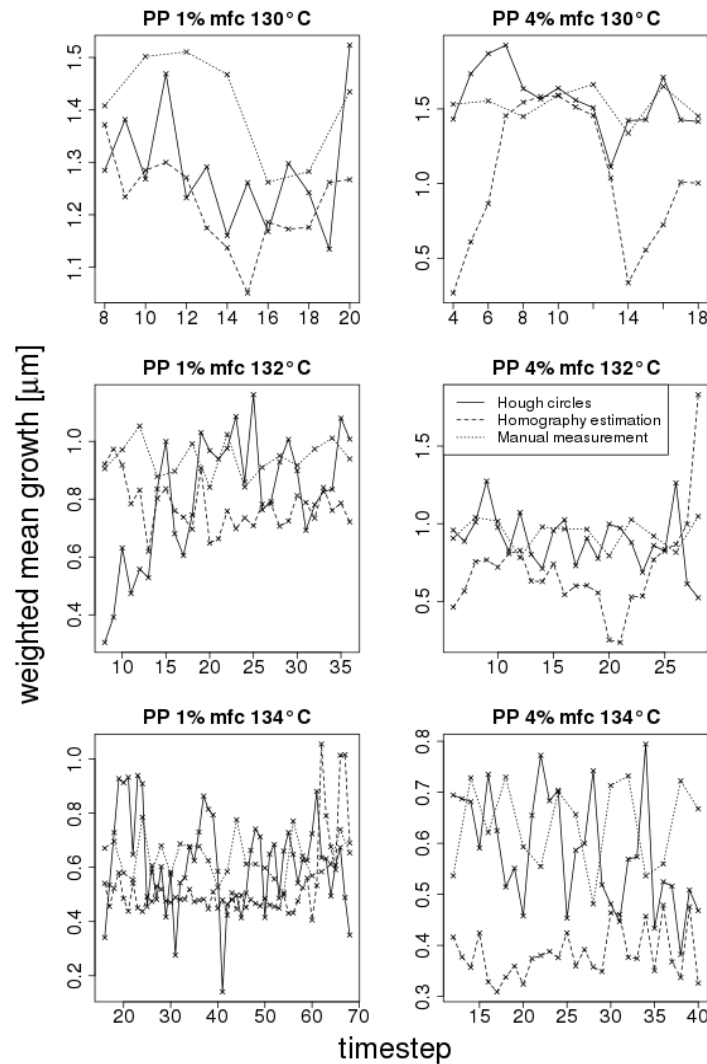


Fig. 3. Results for PP 1% MFC and PP 4% MFC, at the crystallization temperatures of 130°, 132°, and 134°C, respectively.

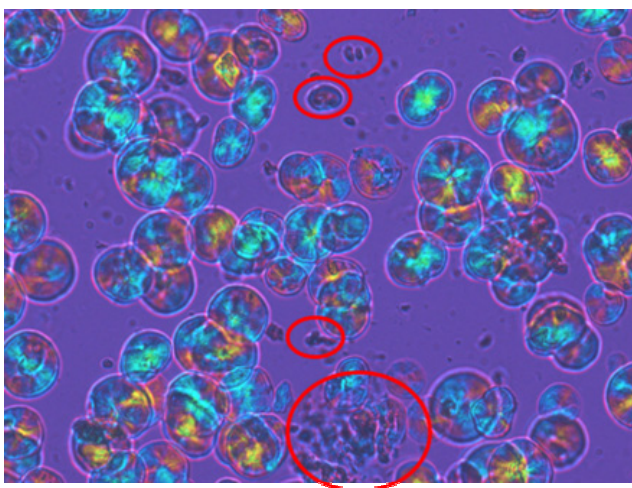


Fig. 4. Frame from a PP 4% MFC sample at crystallization temperature 132°. The indicated agglomerates cannot be identified as spherulites by the Hough transform method.

## DISCUSSION

The reported results show clearly, that quantitative image analysis has the potential to yield reliable growth rate estimates. However, a solution applicable to a wide variety of materials and working properly for high coverage, too, has to be developed. A promising strategy for this seems to be combining the two approaches – object based analysis and time dependent analysis of consecutive frames.

## ACKNOWLEDGMENTS

The authors would like to thank Borealis GmbH, Burghausen, Germany for providing the polypropylene, Prof. Kawees group (Department of Materials Science, Faculty of Science, Chulalongkorn University, Bangkok, Thailand) for the preparation of the MFC, and Michael Godehardt and Benjamin Bauer from

Fraunhofer ITWM for valuable suggestions for the method comparison. We also thank the State Research Center OPTIMAS for supporting the project.

## REFERENCES

- De Santis F, Scermino R, Pantani R, Titomanlio G (2014). Spherulitic nucleation and growth rates in a sheared polypropylene melt. *AIP Conference Proceedings* 1593:294–7
- Hartley R, Zisserman A (2003). *Multiple View Geometry in Computer Vision* (2nd ed.). Cambridge University Press, New York, NY, USA.
- Hernández-Sánchez, F, Carrillo-Escalante, H (2009). A Study of the Kinetics of Polylactic Acid Crystallization by Image Processing. *MRS Proceedings*, 1242. doi: 10.1557/PROC-1242-S4-P102
- Margolin R, Tal A, Zelnik-Manor L (2013). What Makes a Patch Distinct? In *Proceedings of the IEEE Conference on Computer Vision and Pattern Recognition (CVPR '13)*. 2013, IEEE, Washington DC, USA, 1139–46. doi: <http://dx.doi.org/10.1109/CVPR.2013.151>
- Mosaliganti K, Gelas A, Cowgill P, Megason S (2009). An Optimized N-Dimensional Hough Filter for Detecting Spherical Image Objects. *The Insight Journal*, 2009. <http://hdl.handle.net/10380/3129>
- Nomai J, Suksut B, Schlarb AK (2015). Crystallization Behavior of Poly(lactic acid)/Titanium Dioxide Nanocomposites, *KMUTNB Int J Appl Sci Technol* 8:251–8. [dx.doi.org/10.14416/j.ijast.2015.10.003](http://dx.doi.org/10.14416/j.ijast.2015.10.003)
- Plummer CJG, Kausch HH (1995). Real-time image analysis and numerical simulation of isothermal spherulite nucleation and growth in polyoxymethylene. *Colloid Polym Sci* 273:719–32. doi:10.1007/BF00658750
- Stoyan S, Kendall WS, Mecke J (1995). *Stochastic Geometry and its Applications* (2nd ed.). John Wiley & Sons, Chichester-New York-Brisbane-Toronto-Singapore.
- Thanomchat S, Srikulkit K, Suksut B, Schlarb AK (2014). Morphology and crystallization of polypropylene/microfibrillated cellulose composites. *KMUTNB Int J Appl Sci Technol* 7:23–34. [dx.doi.org/10.14416/j.ijast.2014.09.002](http://dx.doi.org/10.14416/j.ijast.2014.09.002)